Clays Clay Miner., Vol. 70, No. 1:72–83, 2022
https://doi.org/10.1007/s42860-022-00177-6

ORIGINAL PAPER

Boron and lithium isotopic signatures of nanometer-sized smectite-rich mixed-layers of bentonite beds from Campos Basin (Brazil)

Norbert Clauer · Lynda B. Williams · I. Tonguç Uysal

Accepted: 18 February 2022

Abstract Boron and lithium were analyzed in three nanometer-sized (<20, 20-50 and 50-100 nm) separates of two Santonian (85.8-83.5 Ma) bentonite samples collected closely in the Campos Basin along the south-eastern Atlantic coast (Brazil). The B and Li data give various trends that suggest varied crystallization conditions for separates that consist of overwhelming smectite with less than 9% illitic layers. The $\delta^{11}B$ of the few illitic tetrahedral sites from one of the samples remains quite constant, while its contents are strictly correlated with those of K, which suggests that illitization proceeded by interaction with pore fluids of the host sediments that supplied the K. In the second sample, the $\delta^{11}B$ of the illite layers from the two coarser fractions is indicative of an early volcanic origin, while the smaller size fraction also interacted with sedimentary fluids. Favored by octahedral substitutions of the smectite layers, the $\delta^{7}Li$ is more strictly regulated by a volcanic link. In turn, the information of the B and Li isotopic compositions and contents from studied mixed-layers suggests a various origin for the few illite layers of the smectite-rich I-S that contain more B than the smectite layers that host more Li. The difference appears to be sample-site and crystal-size dependent, fueled by pore fluids of the hosting turbidites.

Keywords bentonite beds · smectite-rich size separates · nanometer-sized fractions · $\delta^{11}B$ and $\delta^{7}Li$ signatures · smectite and illite authigenesis · Campos Basin (Rio de Janeiro State, Brazil)

N. Clauer (✉)
Institut des Sciences de la Terre et de l'Environnement de Strasbourg, Université de Strasbourg (UdS/CNRS), 67084 Strasbourg, France
e-mail: nclauer@unistra.fr

L. B. Williams
School of Earth & Space Exploration, Arizona State University, Tempe, AZ 85287-1404, USA

I. T. Uysal
Department of Geology, Faculty of Engineering, University of Istanbul-Cerrahpasa, Istanbul, Turkey

Introduction

Isotopic dating of the smectite to illite trend applies to all crystals containing more or less K-bearing layers, according to the kinetic model of the theoretical reaction path (Essene & Peacor, 1995). Their K-Ar and Rb-Sr isotopic systems are controlled by the progressive incorporation of alkalis into the interlayers, illitization being routinely identified by XRD analysis since the mid-1950s (e.g., Burst, 1959; Hower et al., 1976; Środoń & Eberl, 1984; Weaver, 1957). In fact, depending on the solid-state transformation or dissolution/precipitation mechanism of illitization, and assuming that particle-size separation was completed successfully, one might expect different isotopic records for variously sized illite crystals that depend on the host rock and the initial smectite, as well as on the duration and the chemistry of the interacting pore waters. Clauer et al.

(2018) decrypted such illitization processes by analyzing the isotope composition, contents and locations of B and Li in illite layers of smectite-rich mixed-layered illite-smectite (labeled I-S hereafter) by secondary-ion mass spectrometry (SIMS) and nuclear magnetic resonance (NMR) to improve the intimate crystal localization of B. More recently Hindshaw et al. (2019) confirmed the site occupancy of Li in Mg-smectite using Li-NMR. By now and depending on the intrinsic illitization process, the different isotopic trends obtained for nanometer-sized illite crystals of bentonites mostly (e.g., Clauer et al., 1997; Honty et al., 2004) suggest various processes for the smectite-to-illite trend that can potentially be evaluated by analyzing the light-elemental isotopic changes according to the crystal sizes that represent successive growth stages (e.g., Williams et al., 2012).

The bentonite-type rocks do, basically, not contain detrital minerals, unless being somehow bioturbated and contaminated by host sediments on which they were deposited, when the layers were centimeter-thin and when they are subjected to episodic pore-water influxes (e.g., Šucha et al., 1993). Combined with the lack of detrital minerals, this volcanic origin allows the isotopic dating of the authigenic clay minerals that crystallized after deposition (e.g., Baadsgaard et al., 1988; Clauer et al., 2003; Huff, 2008; Samson et al., 1989; Toulkeridis et al., 1998), with complementary information about the chemistry of the interacting fluids. For instance, relative to the initial volcanic material the $^{87}Sr/^{86}Sr$ ratio of the new authigenic crystals can reveal some chemical information about the interacting fluids. This was the case for bentonite layers of the Campos Basin, offshore the Brazilian coast (Clauer et al., 2020), for which ultra-fine nanometer-sized smectite-rich crystals (<20 nm) yield different initial $^{87}Sr/^{86}Sr$ ratios that suggest different crystallization conditions within the same type of diagenetic clay material. This various origin of such identical minerals was the onset of the present study for completing the available information with B and Li isotopic signatures in order, potentially, to identify best the crystallization process with the origin of the interacting fluid carriers. Indeed, B and Li were shown to be informative tracers of clay minerals as B substitutes Si in the tetrahedral sheets, while Li prefers the octahedral sheets. Such exchanges with paleo-fluids can, therefore, trace crystallographic changes as long as the potentially polluting exchangeable interlayer cations are removed (Williams et al., 2012).

The present study was conceived to gain additional information about the smectite-to-illite process by studying an illitization process of a smectite based on the detailed analysis of the B and Li isotopic compositions and contents. Indeed, these B and Li data may depend on the origin of the host rocks and/or on the chemical composition of the interacting fluids. Unfortunately, only two smectite-rich bentonite layers from offshore of Brazil (Fig. 1) were available for these complementary analyses. However, the extracted preliminary information was thought to be of help for future studies, as such bentonite rocks are often selected for studying the smectite to illite trend during low-temperature devitrification of original volcanic ash (Christidis & Huff, 2009). This initial devitrification step includes a diagenetic precipitation of authigenic smectite followed by that of illite when the interacting fluids become K-enriched and the temperature increases during burial (e.g., Altaner et al., 1984; Elliott & Aronson, 1987).

Geological setting

The hosting Campos Basin represents a rift-system of 115,000 km^2 on the southern Brazilian continental margin between 20° and 24°S, with up to 9,000 m of continental to deep-marine sediments interlayered with basalt and ash layers (Mohriak et al., 1990; Fig. 1). Numerous volcanic ash beds were described within the central Upper-Cretaceous sequence of the basin (e.g., Alves et al., 1993; Viana et al., 1998). Between 5 cm and 1 m thick, they occur mostly near the top of sandy layers that are often bioturbated and mixed with the host shales. The associated tectonic activity probably initiated turbidite flows with bentonite layers during Santonian/Campanian time (85.8-83.5 Ma; Caddah et al., 1998) that were buried to about 2,800 m, collected from drill-cores and described in an earlier publication (Clauer et al., 2020). Two of these bentonite layers (named A1 and B1 hereafter) were selected for the study of the B and Li isotopic compositions and contents of their mostly smectite-rich mixed-layer crystals. Unfortunately, the precise geographic location and the detailed stratigraphic age of the samples in the drill-core(s) were not provided.

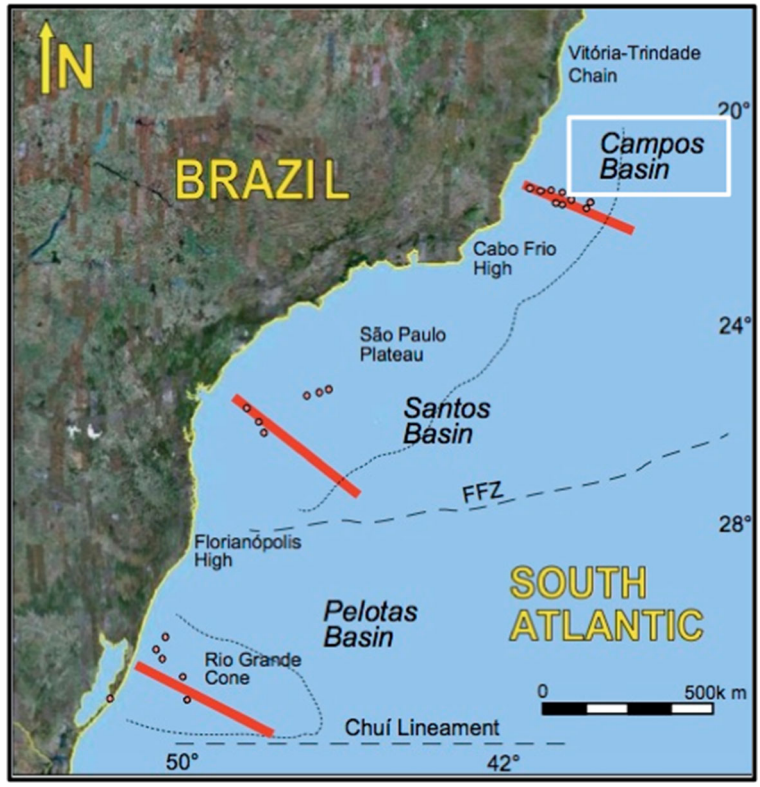

Fig. 1 Map of the southwestern offshore margin of the South Atlantic ocean along the Brazilian continental margin with the location of the Campos Basin. The map was reproduced with the permission of Contreras (2011), its author

Analytical procedure

The analytical procedure was already described in detail (Clauer et al., 2020). Note that the samples were not ground but rather disaggregated by freezing and thawing. Then, the <2 μm fractions of whole-rock smears were recovered by sedimentation in de-ionized water, and treated with ultra-pure sodium-acetate, sodium dithionite and hydrogen peroxide to remove the soluble minerals, the organic matter and the free cations adsorbed on or hosted by the mineral structures (Jackson, 1975). The <0.2 μm fractions were collected by centrifugation and diluted in large amounts of de-ionized water to ensure a so-called "infinite osmotic swelling" (Środoń et al., 1992). Nanometer-sized separates (<20, 20-50 and 50-100 nm) were, then, obtained by continuous, high-speed ultra-centrifugation of the diluted suspensions, and the composition identified and quantified by X-ray diffraction (Table 1).

The B and Li analyses were completed on a Cameca IMS 6f secondary ion mass spectrometer (Williams et al., 2012). Each separate was first rinsed in mannitol, and suspended in 5 μL of de-ionized water filtered through Amberlite resin to remove the aqueous B (Hingston, 1964) and Li (Teichert et al., 2020) before analysis. As the B and Li isotopic compositions and contents of the separates were expected to be quite close, each aliquot was analyzed three times, or more, with an overall analytical precision of $\pm 2\sigma$ (Table 1). A standard (IMt-1 illite) was measured systematically between the analyses of the unknowns to detect and correct the instrumental drift. It is probably useful to recall that B and Li cations stored in the interlayers of smectite are not necessarily in equilibrium with the silicate

Table 1 XRD data of the <20, 20-50 nm size fractions of the selected bentonite samples

Sample IDs	% S in I-S	discrete Illite	Kaolinite
A1a (<20 nm)	92	x	
A1b (20-50 nm)	91	x	
A1c (05-100 nm)	92	xx	
B1a (<20 nm)	94		
B1b (20-50 nm)	96		x
B1c (50-100 nm)	96	x	x

x and xx = traces too small to be amounted

framework (Williams et al., 2007), because they can be introduced at any time after equilibration with the original interacting fluid. Therefore, the exchangeable B and Li of the interlayers were removed before analysis by cation exchange with NH_4Cl (Zhang et al., 1998). Also, as many laboratory chemicals contain contaminating trace amounts of Li, trace-pure reagents were systematically used.

During the previous study of the same size fractions, rock chips and powders were also examined by scanning and transmission electron microscopy. The K contents were measured by flame spectrometry with a solid control of the low K contents detailed by Clauer et al. (2020). The sub-fractions of the A1 and B1 samples were also analyzed for their Rb-Sr isotopic systematics after a supplementary gentle 1N HCl leaching that is known to not alter the Rb-Sr and K-Ar systems of clay materials regardless of crystal type and size, or degree of crystallization (Clauer et al., 1993). After tri-acid digestion of the residues and evaporation of the leachates, the Rb and Sr elements were separated by resin chromatography and analyzed by mass-spectrometry.

Results

A brief review of the previous results

The mineral composition of all analyzed size fractions is dominated by a smectite clay-type (Clauer et al., 2020). Traces of illite were also identified in the fractions, especially in the two coarser A1 ones, while a trace amount of kaolinite was detected in sample B1, too small to be quantified (Table 1). Overall, the different size fractions of both samples consist mostly of smectite-type I-S also containing 8 to 9% illite layers in the A1 separates, and 4 to 6%, in the B1 ones.

Earlier scanning-electron microscopic observations showed irregular crystal surfaces for the ash shards with imprints of coarse 0.1 mm crystals. These rough surfaces were identified as laminar crystal sheets at the edges of the ash particles with perpendicular micrometer-sized lamellar "booklets". At high magnification, the 1-μm platy particles appear oriented, suggesting an interaction with flowing pore fluids that could have fueled the crystallization and growth of the new crystals.

The K-Ar ages confirmed the presence of illite layers in the I-S, some of which being even suspected to have lost radiogenic ^{40}Ar (Clauer et al., 2020). After leaching, the Rb-Sr data points of the untreated (U), leachate (L) and residue (R) aliquots of the three A1 fractions fit individual arrays in an isochron pattern (Fig. 2A). The three A1 data points of the residues also plot along a single array with an age date close to 24 Ma for an initial $^{87}Sr/^{86}Sr$ ratio of ~0.7118. The data points of the B1 fractions give another, more complex pattern with the U-R-L data points of the two finer size fractions fitting two lines with positive slopes, whereas those of the coarsest triplet plot along a line with a negative slope (Fig. 2B). In this case, the $^{87}Sr/^{86}Sr$ ratio of the leachate is higher than that of the corresponding residue, which is unusual for sedimentary materials (Clauer et al., 2011).

The B and Li contents and isotope compositions

In sample A1, the $\delta^{11}B$ remained from 0.9±1.2‰ to 0.3±1.1‰ in the <20 to 50-100 nm aliquots (Table 2), while the B content almost doubled from 34 to 66 μg/g, both being within an analytical uncertainty of <3%. The δ^7Li also did not change beyond analytical uncertainty from 10.5±2.1‰ to 9.4±2.3‰ with increasing crystal size, but with decreasing contents from 120 to 98 μg/g (Table 2; Fig. 3). In sample B1, the $\delta^{11}B$ went lighter from 0.8±0.8 to -4.3±0.7‰ when the particle size increased, while the contents increased from 38 to 58 μg/g. Its δ^7Li remained constant within analytical error at 11.6±3.4‰ with contents increasing from 87 to 104 μg/g in the two coarser size fractions (Table 2; Fig. 3).

As these two elements do not behave strictly the same during illitization with B substituting Si in the tetrahedral site and Li replacing other cations (e.g., Mg) in the octahedral sites, it is appropriate to compare them with the K contents that represent the determining component of the illite interlayers relative to those of smectite-type in the I-S. The $\delta^{11}B$ and B contents of sample A1 are correlated with the K contents and, therefore, are connected. The sketch is different for sample B1, in which K remains quite low and narrow from 0.26 to 0.35%, but which highlights a different behavior for the $\delta^{11}B$ of the smallest <20 nm fraction that is significantly heavier than those of the two other separates (Fig. 3). In turn, differences among the δ^1B and δ^7Li data are obvious in the three fractions of the two samples (Table 2). They need now to be combined into coherent pictures based on the facts that: (1) the coarser A1 fraction

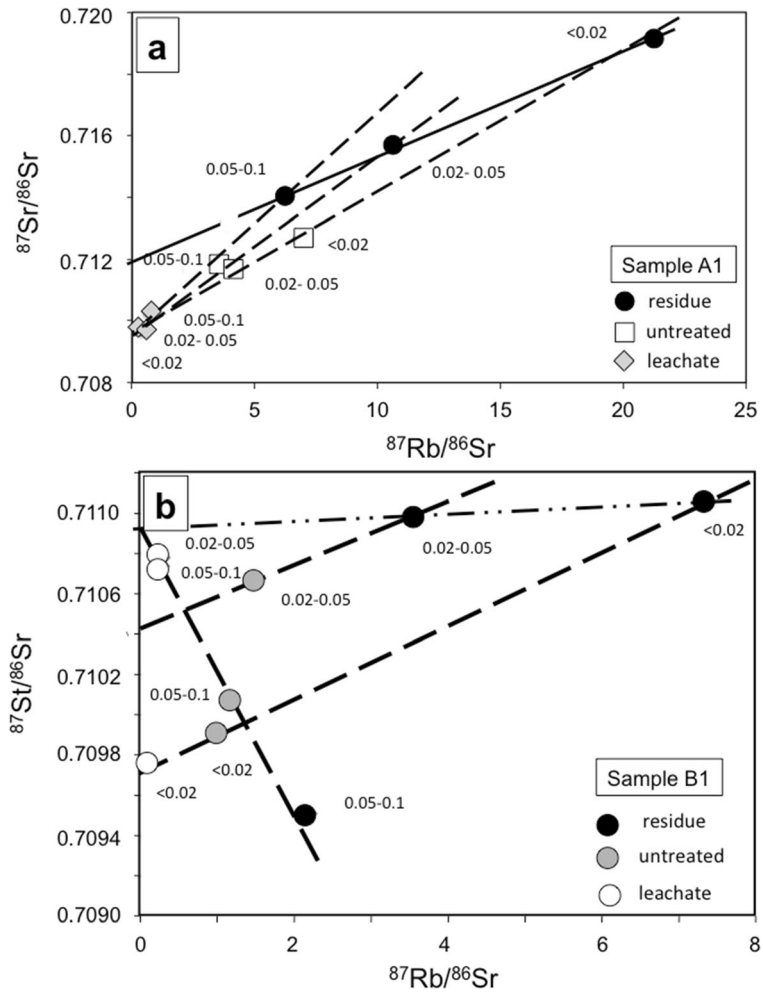

Fig. 2 (a) Rb-Sr data plot of the untreated, leachate and residue separates of each size fractions of sample A1; (b) Rb-Sr data plot of the untreated, leachate and residue separates of each size fraction of sample B1. These diagrams are from Clauer et al. (2020)

contains some illite of probable detrital origin; and (2) the smectite-rich I-S of the coarsest B1 fraction derived from hosting volcanic ash bed, that is to say with no detectable interaction with pore fluids from host sediments.

Discussion

The results, and more precisely the Rb-Sr data already released (Clauer et al., 2020; Table 3), raise concerns about the crystal-chemical conditions and, therefore, the processes occurring during smectitization of the bentonite ash. In turn, they suggest two different processes that will tentatively be evaluated below with the B and Li data.

The thermal history of the bentonite layers

The low content of authigenic illite in the smaller size fractions of the two samples, with an overwhelming smectite content and a parochial amount of kaolinite that can be considered to have no impact on the B and Li signatures, suggests that some K was supplied and fixed when burial temperature increased slightly. The increasing temperature of the bentonite layers apparently reached a maximum value of about 95°C, on the basis of Contreras' (2011) data. Relative to present-day burial, this range allows a theoretical gradient close to 37°C/km for the sedimentary sequence, which is within the 24 to 41°C/km regional spread estimated by Cardoso & Hamza (2014). Therefore, the bentonites were apparently subjected, after deposition, to a moderate diagenetic process powered by a slow and continuous burial.

Table 2 δB, δLi and their contents in the <20, 20-50 and 50-100 nm size fractions of the two analyzed bentonite samples

Sample IDs	$\delta^{11}B$ (+/- 2σ)	B (μg/g) (+/- 2σ)	$\delta^{14}Li$ (+/- 2σ)	Li (μg/g) (+/-2σ)
A1a (<20 nm) average	0.9 (1.2)	34 (1.0)	10.5 (2.1)	120 (21)
analysis 1	1.7 (0.7)	34	11.4 (0.6)	99
analysis 2	-0.2 (0.9)	34	8.4 (0.6)	131
analysis 3	1.3 (0.6)	33	11.7 (0.5)	130
A1b (20-50 nm) average	0.2 (1.6)	60 (2.0)	9.0 (1.4)	117 (2.0)
analysis 1	1.7 (0.6)	59	10.3 (0.5)	117
analysis 2	0.0 (0.6)	62	7.9 (0.6)	116
analysis 3	-1.0 (0.6)	60	8.7 (0.6)	119
A1c (50-100 m) average	0.3 (1.1)	66 (4.0)	9.4 (2.3)	98 (6.0)
analysis 1	1.2 (0.7)	63	8.7 (0.7)	93
analysis 2	0.3 (0.8)	68	7.8 (0.6)	98
analysis 3	-0.6 (0.8)	69	11.6 (0.6)	103
B1a (<20 nm) average	0.8 (0.8)	38 (2.6)	13.2 (0.7)	87 (5.0)
analysis 1	0.7 (0.8)	36	13.7 (0.5)	88
analysis 2	0.1 (0.7)	38	13.2 (0.6)	91
analysis 3	1.4 (0.6)	41	12.5 (0.6)	83
B1b (20-50 nm) average	-4.4 (0.9)	57 (0.5)	9.4 (3.2)	105 (1.0)
analysis 1	-5.3 (0.4)	56	9.4 (0.5)	105
analysis 2	-3.9 (0.4)	57	12.1 (0.3)	104
analysis 3	-4.0 (0.5)	57	6.7 (0.5)	106
B1c (50-100 nm) average	-4.3 (0.7)	58 (0.2)	11.6 (3.4)	102 (1.0)
analysis 1	-4.2 (0.4)	58	9.3 (0.4)	103
analysis 2	-3.6 (0.5)	58	14.9 (0.4)	101
analysis 3	-4.9 (0.5)	58	10.6 (0.5)	101

In summary, the bentonite beds of the Campos Basin underwent a diagenetic event that affected and even dissolved volcanic glass that favored a crystallization of authigenic smectite crystals with a few illite layers that formed either during or after smectite (Clauer et al., 2020). At this point, the isotopic ages obtained do not define an evolution of one continuous or of several periodic diagenetic episodes. The smectite-type layers confirm that the temperature was at the lower limit of the 'illitization window'. Also, the Sr isotopic composition of the leachates systematically higher than that of the seawater during ash deposition and afterwards, excludes an interaction with open seawater, but rather suggests an interaction with evolved pore waters from hosting sediments.

About the contribution of the available Rb-Sr data

On top of a probable mixing of authigenic smectite and detrital illite in, at least, the coarsest A1 fraction, the initial $^{87}Sr/^{86}Sr$ ratios of the U-R-L triplets at 0.70957±0.00024 (2σ) suggests that the crystals of the separates were in contact with pore fluids characterized by a similar $^{87}Sr/^{86}Sr$ ratio that were not of seawater origin, which $^{87}Sr/^{86}Sr$ ratio was of 0.70745±0.00005 (2σ) at deposition time (McArthur et al., 2001). The fact that the data points of the A1 residues plot also along an array with an homogeneous age of 24.3±1.9 Ma (2σ) for an initial $^{87}Sr/^{86}Sr$ ratio of 0.71196±0.00033 (2σ) and not a data scatter does not support the earlier evoked mixing of older minerals with newly formed younger and smaller crystals. If that had been the case, the

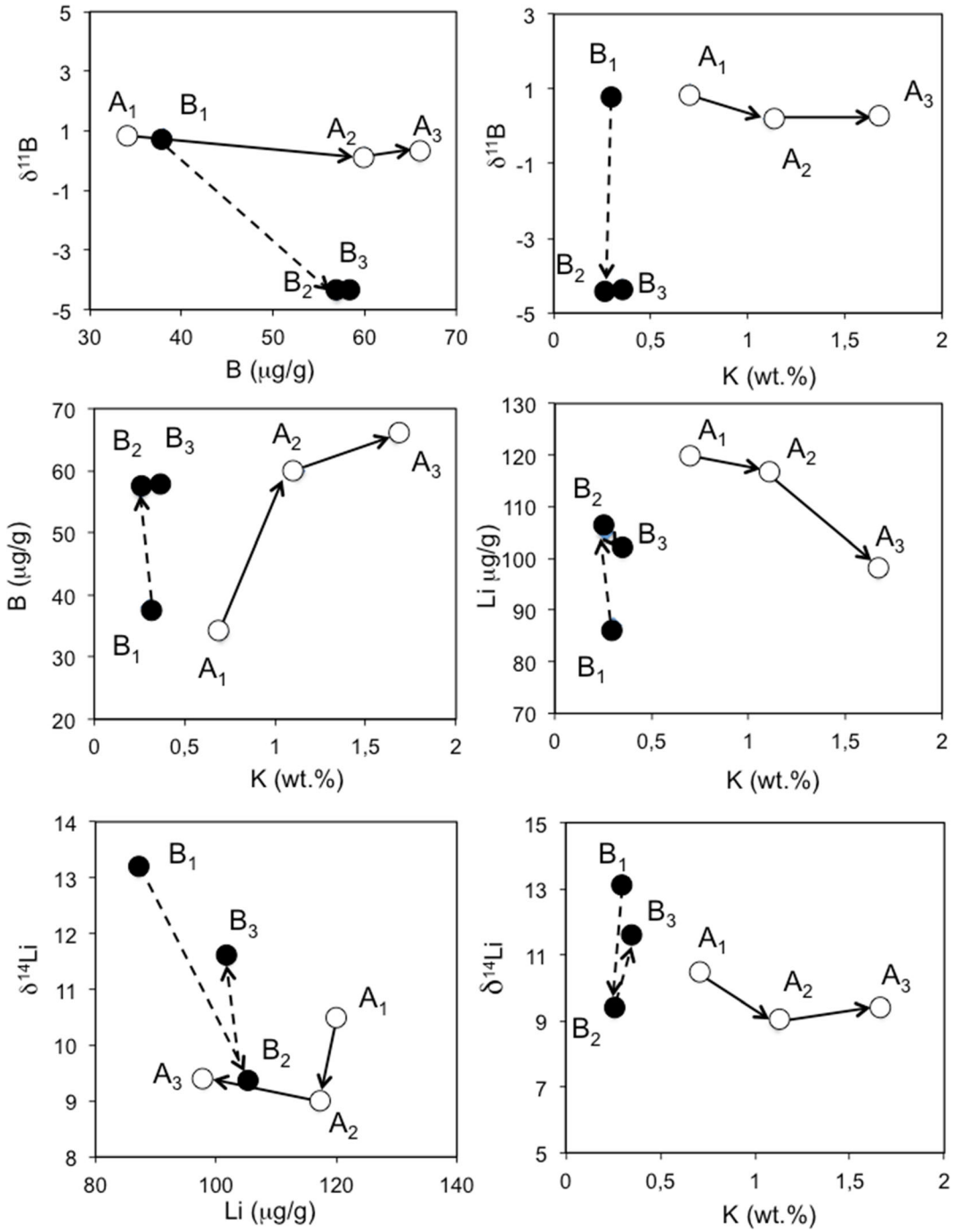

Figure 3 The $\delta^{11}B$ and $\delta^{14}Li$ values and their contents were compared in the three size fractions (<20, 20-50 and 50-100 nm) of the A1 and B1 bentonite samples. They were also compared to the K contents of the same size fractions

individual isotope data should also be plotting along a hyperbolic trend and not a straight line. This 24-Ma line could, then, be an isochron and the age could be of stratigraphic meaning. In this case, the negative slope of the array of the coarse 50-100 nm U-R-L triplet of sample B1 (Fig. 3) is needed to identify the origin of the

Table 3 Rb-Sr data of the untreated, leachate, and residue separates from <20, 20-50, 50-100 nm size fractions of the samples A1 and B1. The data are from Clauer et al. (2020)

Samples	Rb (μg/g)	Sr (μg/g)	Rb/Sr	$^{87}Rb/^{86}Sr$	$^{87}Sr/^{86}Sr$ ($\pm 2\sigma$ in 10^{-6})	K/Rb
A1a (<20 nm) untreated	21.16	9.03	2.343	6.781	0.712667 ± 11	137
leachate	9.40	61.92	0.152	0.439	0.709713 ± 10	
residue	32.07	4.41	7.272	21.08	0.719201 ± 15	
A1b (20-50 nm) untreared	34.06	25.00	1.362	3.943	0.711707 ± 16	136
leachate	13.67	152.5	0.090	0.259	0.709785 ± 10	
residue	37.02	10.12	3.658	10.59	0.715724 ± 10	
A1c (50-100 nm) untreated	45.21	38.26	1.182	3.421	0.711918 ± 10	153
leachate	16.93	137.7	0.123	0.356	0.709748 ± 10	
residue	46.11	21.65	2.130	6.167	0.714054 ± 13	
A1d (100-200 nm) untreated	49.89	60.99	0.818	2.368	0.711724 ± 10	156
leachate	15.43	65.90	0.234	0.678	0.710284 ± 10	
residue	38.60	29.22	1.321	3.825	0.713245 ± 10	
B1a (<20 nm) untreated	6.74	18.25	0.369	1.069	0.709932 ± 10	185
leachate	7.66	136.5	0.056	0.162	0.709791 ± 10	
residue	10.49	4.10	2.559	7.412	0.711070 ± 11	
B1b (20-50 nm) untrearted	7.44	14.41	0.516	1.494	0.710695 ± 10	145
leachate	6.71	58.46	0.115	0.333	0.710800 ± 10	
residue	9.78	7.87	1.243	3.596	0.711012 ± 09	
B1c (50-100 nm) untreated	10.07	24.48	0.411	1.190	0.710087 ± 10	144
leachate	12.12	107.1	0.113	0.328	0.710758 ± 10	
residue	10.90	14.05	0.776	2.245	0.709530 ± 13	
B1d (100-200 nm) untreated	11.19	33.95	0.330	0.963	0.709809 ± 12	144
leachate	11.14	98.81	0.113	0.326	0.710555 ± 10	
residue	12.17	22.72	0.537	1.550	0.709271 ± 11	

illite-type crystals or the illite-consisting I-S layers, and, consequently, the probable interactions with pore fluids of the hosting sediments.

In summary, discrete illitization occurred, either contemporaneously to smectitization or after, due to a limited occurrence of K and Rb supplied by pore fluids from hosting sediments at a temperature also favoring an illite authigenic crystallization. Also, a possible bioturbation effect with the hosting turbidites can also be discarded. In this case, the $^{87}Sr/^{86}Sr$ ratios of the leachates would correspond to values between 0.7106 and 0.7108, which is again higher than that of a contemporaneous marine supply (Jones and Jenkyns 2001), either during ash deposition or during a further smectite and/or illite crystallizations.

What do the B and Li data add to the concept of smectitization and illitization?

It is certainly appropriate to recall that the interpretations evaluated remain somewhat questionable due to the limited number of samples and size fractions that cannot be increased because of a lack of material and of information about the geographic location and the sampling. On the other hand, B and Li isotopic studies of nanometer-sized smectite-rich separates from various bentonite beds are already available (e.g., Clauer et al., 2018; Martos-Villa et al., 2020; Williams et al., 2013). In the East Slovak Basin, their contents of illite crystals record variations of interacting fluids, while their isotopic ratios are a function of the temperature and fluid

isotopic compositions (Clauer et al., 2014). Also, illite-rich separates of bentonites from the same basin yield low B contents (30-100 μg/g) with a $\delta^{11}B$ that decreases from −5 to −17‰ as the B contents increase. In the case of smectite components from bentonites worldwide, the non-exchangeable B concentrations vary widely from 0.2 to 196 μg/g (Köster et al., 2019). Most of these smectite crystals also contain small amounts of interstratified illite that requires a varied fluid-mineral B partition. In turn, the $\delta^{11}B$ values of the structural B from tetrahedral smectite sites range from −30.1‰ to +12.2‰.

The smectite-rich A1 fractions, for which the K content is very low and narrowly spread, contain illite layers that might be of two origins: mainly diagenetically authigenic in the finer fraction, or detrital of either sedimentary or volcanogenic origin in the coarser fraction. Here, these fractions show no trend in their $\delta^{11}B$ values with an average of 0.63±1.0‰ for three analyses of each fraction (n=9). In contrast, there is an increase in the B-content relative to grain size, from 34 μg/g in the finest to 66 μg/g (n=3) in the coarsest fraction. This increase with constant $\delta^{11}B$ suggests that the chemical composition of the fluids did not change markedly while contributing to the crystal growth. However, as more B was incorporated the volume of the illite had to increase, which needed also additional K. The selection of the two A1 and B1 samples was two-fold, one resulting supposedly from a different crystallization processes than the second with different $\delta^{11}B$ and B trends. The obtained various results suggest that either: (1) temperature increased (assuming the same pore-fluid composition), which decreased the B isotope fractionation ($\Delta_{min\text{-}water}$); or (2) a fluid carrying a lighter $\delta_{11}B$ equilibrated with the coarser I-S fractions, assuming a constant temperature. As the two samples were collected quite close to each other, the second hypothesis seems more appropriate, being applicable to both samples.

The $\delta^{7}Li$ of the three A1 fractions averages +9.6±1.6‰ (n=9) with a content of 112±15 μg/g. Both values are statistically within analytical uncertainty, suggesting again that the illite layers of the smectite-rich size separates formed in equilibrium with a chemically stable fluid, the initial crystals forming with a minimal change in the burial temperature. Similarly, the δ^{7} Li of the three B1 size fractions yields no significant trends with crystal growth at an average of +11.4 ±2.6 ‰ (n=9) and a content of 98±8 μg/g, both again within analytical uncertainty. This reasoning begs the question of how one can obtain a change in B without a concomitant change in Li if the minerals precipitated from the same source fluid. One possibility is that there was a mixing with a fluid enriched in B, but not in Li, which may account for the increased B content in the coarser B1 samples, together with a progressively lighter composition for $\delta^{11}B$ (-4‰). Once more, the isotopically light samples might still include the detrital illite from outside the bentonite, e.g. from host sediments.

How to integrate the B and Li isotopic trends and the Rb-Sr data

One issue still needs to be addressed, namely the overwhelming occurrence of smectite-rich I-S in the bentonite layers mostly resulting from initial alteration of the volcanic ash, together with low contents of illite layers, while it is not clear yet if the K that generated the illite layers occurred while the smectite interlayers were forming, or later when the temperature was more adequate for a crystallization of illite layers. There is yet no undisputable argument by the K-Ar and Rb-Sr isotopic dating methods as they apply solely to minerals or crystal interlayers having fixed K and Rb its sister element. The only age references are from illite layers, even if they represent less than 10% of the overall smectite-rich particles. One aspect of the process is that the very low content of radiogenic ^{40}Ar, and even its lack in some of the smallest nanometer-sized separates, suggests that illitization could have occurred delayed relative to smectitization, lasting even until present-day.

The $\delta^{11}B$ remains almost constant in the A1 fractions relative to a continuously increasing K content with size, strongly suggesting that the illite content in the smectite-type interlayers is related to crystal size. This constant $\delta^{11}B$ relative to an increasing K content indicates that the fluids had to remain identical in composition and at an almost constant temperature during illite growth; the K increase following the overall crystal growth. The $\delta^{7}Li$ yields a different trend with relatively similar data for the two coarser fractions, which is confirmed by the same $\delta^{7}Li$ values relative to the K content. Therefore, if the illite crystals of the coarsest A1 fraction had different $\delta^{11}B$ and $\delta^{7}Li$ than those of the two finer fractions, one cannot exclude that identified as possibly detrital, they are of sedimentary origin with earlier crystallization conditions that could have been similar to those of the later fine illite crystals. In turn, they should then be considered as early authigenic precipitates of volcanic

origin, rather than detrital contaminants from hosting turbidites.

The Rb-Sr data suggest also a different origin for the coarsest B1 fraction, mostly volcanic on the basis of the specific spread of the U-R-L data points in an isochron diagram. This hypothesis is supported by the lower $^{87}Sr/^{86}Sr$ ratio of the coarsest residue than that of its corresponding leachate. In addition, the $\delta^{11}B$ and B contents of that coarser fraction are closer to those of the intermediate size fraction than to those of the finest fraction. They are also close to those of sample A1, which crystals probably interacted with pore fluids of sedimentary origin. The K contents varying only very slightly among the three B1 fractions, the $\delta^{11}B$ and B contents may then depend on the size and nature of the crystals. In this context, the $\delta^{7}Li$ values that are quite distinct from each other, may relate to the overwhelming occurrence of smectite, as are the $\delta^{7}Li$ values relative to the K contents.

The Rb-Sr data of the U-R-L aliquots from the two finer B1 fractions plot along sub-parallel lines with initial $^{87}Sr/^{86}Sr$ ratios of about 0.70972 for the finer fraction to about 0.71045 for the intermediate fraction, while the data of the coarser size fraction fit a three-point line ending at an even higher initial of 0.71095 (Fig. 2). It looks like the overwhelming smectite interacted with fluids characterized by an $^{87}Sr/^{86}Sr$ ratio apparently representative of a volcanic Sr isotopic value characteristic of an acidic origin. Interestingly, the line joining the data points of the smallest and intermediate residues in an isochron diagram also yields an initial $^{87}Sr/^{86}Sr$ value of about 0.71095 (Fig. 2). It is, therefore, plausible that during crystallization of the finer smectite crystals within the volcanic ash, the amount of the interacting pore fluids increased progressively with a stable $^{87}Sr/^{86}Sr$ signature. Such an evolution explains the distribution of the $\delta^{11}B$ with the data of the intermediate and coarse B1 fractions closer to each other than to that of the finer crystals. This differential interaction seems not to have affected the $\delta^{7}Li$ with fairly grouped Li contents representative of continuously growing smectite, which suggests a volcanic contribution in the coarser residue and no change in the impact of the pore fluids on the smaller crystals.

In summary, the $\delta^{11}B$ and $\delta^{7}Li$ values, together with the corresponding B and Li contents of the A1 and B1 size fractions, are varied despite a close location that point to different origins and/or different crystallization conditions. The constant $\delta^{11}B$ for the increasing crystal size in sample A1 suggests a stable composition for the interacting pore fluids from sedimentary host rocks, at a likely stable low burial temperature. The case of sample B1 with a different $\delta^{11}B$ for the two coarser fractions supports the hypothesis of interacting fluids with a constant $\delta^{11}B$ value for the finer crystals, not for the coarser, which maintained the imprint of the volcanic precursors. For Li, the finest and the coarsest B1 fractions yield heavier $\delta^{7}Li$ values than the three separates of sample A1 with only a lower Li content for the finest fraction. As an interaction with seawater can be discarded, the decrease in $\delta^{7}Li$ could reflect an influx of hydrocarbon-polluted fluids (Williams et al., 2013; Clauer et al., 2022), in an oil-producing region, as is the case here. Indeed, the $\delta^{7}Li$ decrease does not coincide with a constant low K content and, therefore, does not seem to be part of the illitization trend. It rather reflects changing origins for the constitutive crystals that necessarily involve changing pore fluids. The zigzaging variation in the $\delta^{7}Li$ of the three B1 fractions with the lower value for the intermediate fraction is probably due to the dominant volcanic original reference in the coarser fraction combined with a variable impact of external pore fluids during further crystallization of the fine crystals.

Conclusions

Santonian (85.8-83.5 Ma) nanometer-sized (<20, 20-50 and 50-100 nm) bentonite separates buried presently to approximately 2,800 m in the Campos Basin located offshore the Rio de Janeiro State (Brazil), were studied here for their $\delta^{11}B$ and $\delta^{7}Li$ compositions, and B and Li contents. In contrast to previous similar mineralogical, chemical, and isotopic studies of nanometer-sized illite-rich mixed layers or pure illite crystals of such kind of bentonite layers, the aim here was to decrypt how illite crystals initiate, either during or after alteration of the initial volcanic ash into smectite, at a burial temperature below 95°C and interacting probably with pore fluids from hosting turbidites.

The smectite-rich mixed layers of sample B1 contain remnants of initial volcanic ash, while illitization remained limited mainly due to a limited supply of alkali elements and partly to the low burial temperature. The

$\delta^{11}B$, $\delta^{7}Li$, and B and Li contents of the three size fractions from the two studied samples are quite varied. In the case of sample A1 hosting some illite of plausible early volcanic origin in the coarser fraction, the $\delta^{11}B$ is constant relative to the size fractions, while its $\delta^{7}Li$ is widely spread, as are the contents of both B and Li. Progressive interactions with pore fluids from hosting turbidites could also be detected, while the crystals grew. Conversely, the repartitions in the coarser size separate of the second B1 sample are different than in the two finer fractions that yield similar B and Li contents suggesting extensive interactions with sedimentary pore fluids, while the coarsest fraction retained some of its initial volcanic signature.

Acknowledgements We would like to thank Drs. D.B. Alves and F. Pellon de Miranda of the Brazilian Research Development Center (CENPES) for the sample supply, as well as the geographic, stratigraphic information and constructive discussions. The SIMS analyses for B and Li isotopic compositions were conducted at the Arizona State University SIMS Facility supported by the US National Science Foundation grant EAR 1819550. Two reviewers are also sincerely thanked for their comments.

Authors' contributions Conceived by Norbert Clauer, performed and written by all authors

Funding US National Science Foundation grant EAR 1819550.

Availability of data and material EarthChem Repository; ASU Repository

Code availability Not applicable

Declarations

Ethics approval Not required

Consent to participate Not applicable

Consent for publication Approved by all authors

Conflict of interest On behalf of all authors, the corresponding author states that there is no conflict of interest.

Availability of data and material As above

Funding As above

REFERENCES

Altaner, S. P., Hower, J., Whitney, G., & Aronson, J. L. (1984). Model for K-bentonite formation: Evidence from zoned K-bentonites in the Disturbed Belt, Montana. *Geology, 12*, 412–425.

Alves D. B., Mizusaki A. M. P. & Caddah L. E. G. (1993) Camadas de cinzasvulcanicas no Santoniano (Creticeo Superior) da Bacia de Campos. Simposio de Geologia do Sudeste, 3, Rio de Janeiro, SBG, Atas, 37-42.

Baadsgaard, H., Lerbekmo, J. F., & McDougall, I. (1988). A radiometric age for the Cretaceous–Tertiary boundary based upon K–Ar, Rb–Sr, and U–Pb ages of bentonites from Alberta, Saskatchewan, and Montana. *Canadian Journal of Earth Sciences, 25*, 88–106.

Burst, J. F. (1959). Post diagenetic clay mineral-environmental relationships in the Gulf Coast Eocene in clays and clay minerals. *Clays and Clay Minerals, 6*, 327–341.

Caddah, L. F. G., Alves, D. B., & Mizusaki, A. M. P. (1998). Turbidites associated with bentonites in the Upper-Cretaceous of the Campos Basin, offshore Brazil. *Sedimentary Geology, 115*, 175–184.

Cardoso R. A. & Hamza V. M. (2014) Heat flow in the Campos sedimentary basin and thermal history of the continental margin of southeast Brazil. ISRN Geophysics, Hindawi Publication Corporation Article ID 384752, 19 pages

Christidis, G., & Huff, W. (2009). Geological aspects and genesis of bentonites. *Elements,5,* 93–98. https://doi.org/10.2113/gselements.5.2.93

Clauer, N., Chaudhuri, S., Kralik, M., & Bonnot-Courtois, C. (1993). Effects of experimental leaching on Rb-Sr and K-Ar isotopic systems and REE contents of diagenetic illite. *Chemical Geology, 103*, 1–16.

Clauer, N., Środoń, J., Francù, J., & Šucha, V. (1997). K-Ar dating of illite fundamental particles separated from illite/smectite. *Clay Minerals, 32*, 181–196.

Clauer, N., Liewig, N., Pierret, M. C., & Toulkeridis, T. (2003). Crystallization conditions of fundamental particles from mixed-layers illite-smectite of bentonites based on isotopic data (K-Ar, Rb-Sr and $\delta^{18}O$). *Clays and Clay Minerals, 51*, 664–674.

Clauer, N., O'Neil, J. R., Honnorez, J., & Buatier, M. (2011). $^{87}Sr/^{86}Sr$ and $^{18}O/^{16}O$ ratios of clay minerals from a hydrothermal mound near the Galapagos rift as records of origin, crystallization temperature and fluid composition. *Marine Geology, 288*, 32–42.

Clauer, N., Honty, M., Fallick, A. E., Šucha, V., & Aubert, A. (2014). Regional illitization in bentonite beds from East Slovak Basin based on isotopic characteristics (K-Ar, δ O and δD) of illite-type nanoparticles. *Clay Minerals,49,* 247–275.

Clauer, N., Williams, L., Lemarchand, D., Florian, P., & Honty, M. (2018). Illitization decrypted by B and Li isotope geochemistry of nanometer-sized illite crystals of bentonite beds from East Slovak Basin. *Chemical Geology, 477*, 177–194.

Clauer, N., Środoń, J., Aubert, A., Uysal, I. T., & Toulkeridis, T. (2020). K-Ar and Rb-Sr dating of nanometer-sized smectite-rich mixed-layers from bentonite beds of the Campos Basin (Rio de Janeiro State, Brazil). *Clays and Clay Minerals, 68*, 446–464.

Clauer, N., Williams, L. B., & Fallick, A. E. (2022). Tracing organic-inorganic interactions by light stable isotopes (H, Li, B, O) of an oil-bearing shale and its clay fraction during hydrous pyrolysis. *Clays and Clay Minerals,* in press.

Contreras J. (2011) Seismo-stratigraphy and numerical basin modeling of the southern Brazilian continental margin (Campos, Santos and Pelotas basins). PhD thesis, University Heidelberg, Germany, 146 p.

Elliott, W. C., & Aronson, J. L. (1987). Alleghanian episode of K-bentonites illitization in the southern Appalachian Basin. *Geology, 15*, 735–739.

Essene, E. J., & Peacor, D. R. (1995). Clay mineral thermometry - a critical prospective. *Clays and Clay Minerals, 43*, 540–553.

Hindshaw, R. S., Tosca, R., Goût, T. L., Tosca, N. J., & Tipper, E. T. (2019). Experimental constraints on Li isotope fractionation during clay formation. *Geochimica et Cosmochimica Acta, 250*, 219–237.

Hingston, F. J. (1964). Reactions between boron and clays. *Australian Journal of Soil Research, 2*, 83–95.

Honty, M., Uhlík, P., Šucha, V., Caplovicová, M., Francù, J., Clauer, N., & Biron, A. (2004). Smectite to illite alteration in salt-bearing bentonites (The East Slovak Basin). *Clays and Clay Minerals, 52*, 533–551.

Hower, J., Eslinger, E. V., Hower, M., & Perry, E. A. (1976). Mechanism of burial metamorphism of argillaceous sediments. 1. Mineralogical and chemical evidence. *Geological Society of America Bulletin, 87*, 725–737.

Huff, W. D. (2008). Ordovician K-bentonites: Issues in interpreting and correlating ancient tephras. *Quaternary International, 178*, 276–287.

Jackson M. L. (1975) Soil chemical analysis – advanced course. Madison, Wisconsin 386p.

Jones, C. E., & Jenkyns, H. C. (2001). Seawater strontium isotopes, oceanic anoxic events, and seafloor hydrothermal activity in the Jurassic and Cretaceous. *American Journal of Sciences, 301*, 112–149.

Köster, M. H., Williams, L. B., Kudejova, O., & Gilg, H. A. (2019). The boron isotope geochemistry of smectites from sodium, magnesium and calcium bentonite deposits. *Chemical Geology, 12035*.

Martos-Villa, R., Mata M. P., Williams L. B., Nieto F., Arroyo Rey X. & Sainz-Diaz C. I. (2020) Evidence of hydrocarbon-rich fluid interaction with clays: Clay mineralogy and boron isotope data from gulf of cádiz mud volcano sediments. *Minerals10*, 651. https://doi.org/10.3390/min10080651

McArthur, J. M., Howarth, R. J., & Bailey, T. R. (2001). Strontium isotope stratigraphy: LOWESS Version 3: Best fit to the marine Sr-isotope curve 0-509 Ma and accompanying look-up table for deriving numerical age. *Journal of Geology, 109*, 155–170.

Mohriak, W. U., Mello, M. R., Karner, G. D., Dewey, J. F., & Maxwell, J. R. (1990). Structural and stratigraphic evolution of the Campos Basin, offshore Brazil. In A. J. Tankard & H. R. Balkwill (Eds.), *Extensional tectonics and stratigraphy of the North Atlantic margins*. American Association of Petroleum Geologists Memoir (Vol. 46, pp. 577–598).

Samson, S. D., Patchett, P. J., Roddick, J. C., & Parrish, R. R. (1989). Origin and tectonic setting of Ordovician bentonites in North America: Isotopic and age constraints. *Geological Socieyu of America Bulletin, 101*, 1175–1181.

Środoń J. & Eberl D. D. (1984) Illite. In: Bailey S.W. (Ed.), Mineralogical society of america, reviews in mineralogy 13, Washington, DC, 584 p.

Środoń, J., Elsass, F., McHardy, W. J., & Morgan, D. J. (1992). Chemistry of illite/smectite inferred from TEM measurements of fundamental particles. *Clay Minerals, 27*, 137–158.

Šucha, V., Kraus, I., Gerthofferová, H., Peteš, J., & Sereková, M. (1993). Smectite to illite conversion in bentonites and shales of the East Slovak Basin. *Clay Minerals, 28*, 243–253.

Teichert, Z., Bose, M., & Williams, L. B. (2020). Lithium isotope compositions of U.S. coals and source rocks: Potential tracer of hydrocarbons. *Chemical Geology, 549*, 119694.

Toulkeridis, T., Clauer, N., Chaudhuri, S., & Goldstein, S. L. (1998). Multi-method (K-Ar, Rb-Sr, Sm-Nd) dating of bentonite minerals from eastern United States. *Basin Research, 10*, 261–270.

Viana, A. R., Faugères, J. C., Kowsmann, R. O., Lima, J. A. M., Caddah, L. F. G., & Rizzo, J. G. (1998). Hydrology, morphology and sedimentology of the Campos continental margin, offshore Brazil. *Sedimentary Geology, 115*, 133–157.

Weaver, C. E. (1957). The clay petrology of sediments. *Clays and Clay Minerals, 6*, 154–187.

Williams L. B., Clauer N. & Hervig R. L. (2012) Light stable isotope microanalysis of clays in sedimentary rocks. In: Sylvester P. (Ed.) Quantitative mineralogy and microanalysis of sediments and sedimentary rocks. Mineralogical Association of Canada, Short Course 42, 55-73.

Williams, L. B., Środoń, J., Huff, W. D., Clauer, N., & Hervig, R. L. (2013). Light element distributions (N, B, Li) in Baltic Basin bentonites record organic sources. *Geochimica et Cosmochimica Acta, 120*, 582–599.

Williams, L. B., Turner, A., & Hervig, R. L. (2007). Intracrystalline boron isotope partitioning in illite-smectite: Testing the geothermometer. *American Mineralogist, 92*, 1958–1965.

Zhang, L., Chan, L. H., & Gieskes, J. M. (1998). Lithium isotope geochemistry of pore waters from Ocean Drilling Program Sites 918 and 919, Irminger Basin. *Geochimica et Cosmochimica Acta, 62*, 2437–2450.